The effect of swingarm stiffness on motorcycle stability: experimental measurements and numerical simulations

Luca Taraborrelli

Department of Industrial Engineering

University of Padova

Via Venezia 1, 35131, Padova, Italy

e-mail: luca.taraborrelli@yahoo.it

Valerio Favaron

Department of Industrial Engineering

University of Padova

Via Venezia 1, 35131, Padova, Italy

e-mail: valeriofavaron90@gmail.com

Alberto Doria

Department of Industrial Engineering

University of Padova

Via Venezia 1, 35131, Padova, Italy

e-mail: alberto.doria@unipd.it

*Corresponding author

Abstract: This paper focuses on the effect of swingarm deformability on motorcycle stability and in particular on the weave mode. Multibody models for the analysis of stability and handling of single track vehicles require a lumped element representation of the deformability of the critical structural elements of the vehicle. The twist axis method is used to identify lumped stiffness and damping elements able to represent bending and torsion deformability of the swingarm. Experimental tests and identification results dealing with two different swingarms are presented. The identified lumped stiffness and damping elements are implemented in a multibody code and some numerical stability analyses are carried out. Calculated results show that swingarm deformability has a small effect on the stability of super sport motorcycles,

whereas the stability of the weave mode of enduro motorcycles is affected by swingarm deformability in a specific range of speeds.

Keywords: motorcycle, swingarm, weave, stability, twist axis, identification.

Biographical notes: Luca Taraborrelli graduated in Clinical Engineering in 2010 and he finished the Master's degree in Biomedical Engineering in 2012 at the University of Rome "La Sapienza". Successively, he achieved a Doctorate degree in Mechanical Engineering at the University of Padova with a thesis on the "Identification and improvement of the dynamic properties of the components of two-wheeled vehicles". In the framework of his PhD, he has been co-author of some publications in international journals and conference proceedings, collecting two "Best Paper Awards" at the ASME AVT 2014 and ASME AVT 2016 conferences. The research fields in which he is expert and passionate are biomechanics, mechanical vibrations and vehicle dynamics.

Valerio Favaron achieved his master degree at the University of Padua in March 2015 with a thesis dealing with the effect of tyres inflation pressure on motorcycle stability, supervised by Professor Vittore Cossalter. Then, he was employed as a researcher at the Motorcycle Dynamics Research Group at the University of Padua. His field of expertise is related to the study of instability of two wheeled vehicle in particular referring to motorcycle weave and wobble.

Alberto Doria received the Laurea degree in Mechanical Engineering (with honors) from the University of Padova in 1984. In 1986 he joined the Italian Research Authority as contract researcher, becoming member of the design group of RFX, a fusion experiment funded by Euratom. He designed and developed the manipulator of the RFX machine. He received in 1987 the degree "Corso di Perfezionamento in Ingegneria del Plasma e della Fusione Termonucleare Controllata" from the University of Padova. In 1990 Alberto Doria joined the University of Padova as researcher of Mechanics of Machines. His research activity was in the fields of robotics and control of vibrations and noise. He developed particular Helmholtz resonators that were implemented in an air-conditioner. In 1997 Alberto Doria joined the Motorcycle Dynamics Research Group of Padova University. He begun a research activity in the field of two wheeled vehicles that included modeling, simulation and experimental issues. In 2002 Alberto Doria became Associate Professor of Mechanics of Machines at the University of Padova. The current research activities of Alberto Doria are: development of light vehicles for sustainable mobility; modal analysis and identification; vibration energy harvesting. In 2014 Alberto Doria has obtained the national qualification needed for becoming full professor. Alberto Doria is author of 123 scientific publications and has been responsible for research projects and contracts with companies. Alberto Doria is member of ASME.

---

1 Introduction

Stability and handling of motorcycles are strongly influenced by the typical modes of vibration of this class of vehicles. In particular the weave and wobble modes are the main concerns of designers and engineers. Wobble is a high frequency mode (8÷10 Hz), which chiefly involves the rotation of the front frame about the steer axis, whereas weave is a low frequency mode (1÷4 Hz), which involves the whole vehicle with relevant roll, yaw and steer rotations and lateral displacement of the rear frame [1] [2].

The basic mathematical model for studying handling and stability has 4 degrees of freedom (DOF) associated with steer, roll, yaw and lateral displacement and has to include at least a linear tire model with relaxation properties [2].

In recent years, owing to the development of multibody codes, a relevant progress has been made in the study of stability of single track vehicles.

Stability in cornering and during acceleration/braking has been studied [3] surpassing the limits of the first studies, which dealt with linear stability about straight running motion at constant speed.

Many improvements of the model of the system have been made. The rider is an important part of the system, since his/her mass is an important share of the total mass, modern multibody models take into account steer impedance due to the rider's arms [4], bending and torsion deformability of the rider's body [5]. In [6] the kinematics of the vehicle has been improved taking into account the actual point of contact of toroidal tires. Improvements in the description of tire deformability and relaxation properties have been made in [7] and [8].

Rather early riders and engineers discovered that the stiffnesses of front fork, swingarm and chassis play an important role in motorcycle stability. After the first studies of Sharp and Alstead [9] further improvements have been made by introducing in the multibody codes lumped stiffness elements to represent the critical stiffness of the structural elements of motorcycles [10] [11].

The improvement of knowledge of motorcycle stability and handling has required not only a research effort in the fields of modeling and numerical methods, but also a research effort in the fields of experimental methods and identification [12] in order to identify the mechanical properties of tires, structural components and riders that are needed by advanced multibody codes.

This paper focuses on the effect of swingarm stiffness and damping properties on motorcycle stability, since this aspect has been scarcely addressed by previous research papers.

The first part of the paper deals with the identification of the stiffness and damping properties of swingarms. Actually a swingarm is a continuous system, but a lumped element representation of stiffness and damping properties is needed to model the structural-dynamic behavior of the swingarm in a multibody code. In order to define the values and the position of the lumped stiffness and damping elements, the twist axis approach is adopted.

The twist axis was first introduced by Giles and Sharp in 1982 [13] and it was defined as the intersection between the symmetry plane of the vehicle and the plane of the wheel (front or rear) in loaded condition. A rotation about the twist axis causes a displacement and a rotation of the wheel equal to the ones caused by the actual compliance of the structural element that supports the wheel. Static tests make it possible to identify the static twist axis and twist stiffness, which is the rotational stiffness about the twist axis. In this paper, by means of dynamic tests, the twist axes of the bending and torsion modes of the swingarms are identified as well and, then, twist stiffness is decomposed into the bending and torsion components. Therefore, information about swingarm deformability that takes into account the modal properties of the component is obtained.

The second part of the paper deals with the effect of swingarm deformability on motorcycle stability. The lumped element representation of swingarm stiffness and damping obtained by means of the twist axis approach is introduced in the multibody model of two motorcycles and analyses are carried out to highlight the effect of swingarm characteristics on motorcycle stability.

2 Experimental equipment and tests

Two swingarms have been tested in the framework of this research. The first swingarm is mounted on super-sport motorcycles, presents a bulky and compact design and its weight is 6.96 kg. The second swingarm, on

the contrary, is designed for enduro motorcycles, it is characterized by a simple geometry and its weight is 5.45 kg. Both swingarms are made of aluminum alloys. During the experimental tests, a fake spindle has been mounted on the rear wheel hub of the swingarms in order to avoid unrealistic motions between the two arms.

2.1 Testing equipment and methods

The measurement of stiffness has been carried out on the specific testing rig of the University of Padova, which is shown in Figure 1. It consists of a stiff column, a servo-hydraulic actuator, and a system of sensors. The column is clamped to a grooved plate and is equipped with metal jaws which make it possible to constrain the motorcycle swingarm by locking the swingarm pivot. During the tests, the stem of a hydraulic actuator is connected with two ball-and-socket joints to the rear wheel hub of the swingarm and excites the swingarm in the lateral direction. The actuator is powered by a hydraulic unit, and can produce a static force up to 5000 N. A load cell aligned with the actuator axis is used to measure the force applied by the actuator. The measurement system includes three laser sensors that are used to measure the motion of the component under test. The laser sensors have a measurement range of 20 mm and a max resolution of 4 μm.

This testing rig is used to carry out static tests, which aim to identify the twist stiffness and the deformation pattern of the swingarm (described by means of the static twist axis) when a static load is applied to the rear wheel hub. In more detail, the position of the static twist axis is identified monitoring the motion of a metal reference plate that is stiffly attached to the swingarm close to the force's application point. The motion of the plate is measured by means of the laser sensors and the outputs of the three lasers are employed for calculating the equation of the plane defined by the metal plate in the loaded and unloaded conditions. From the intersection between two planes, it is possible to identify the position of the static twist axis.

The described method corresponds to a more general definition of the twist axis as well. When a nearly 2D structure (like a swingarm) has an end fixed and an end loaded on one side by an out-of-plane force, a stiff reference plate clamped to the other side of the loaded end of the structure follows the motion of the loaded end of the structural element and behaves like a rigid body. For this reason the basic concepts of rigid body mechanics can be adopted to study the motion of the reference plate. An important result of rigid body mechanics is that a generic differential spatial rigid motion can be considered an helical motion about an axis that coincides with the twist axis defined as the intersection between unloaded and loaded planes [14].

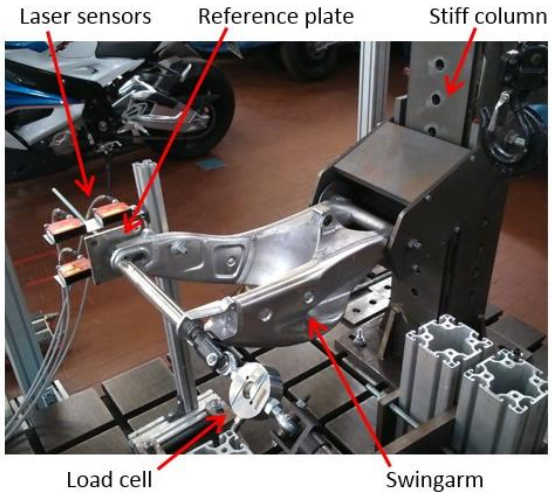

Figure 1. Picture of the testing rig.

The displacement of the force's application point in the lateral direction (y_{lat}) can be calculated from the equation of the reference plane in the loaded condition. The lateral stiffness is defined as:

$$k_{lat} = \frac{F}{y_{lat}} \qquad (1)$$

Lateral displacement y_{lat} can be expressed also as a function of twist angle ϑ_{tw} and twist arm a_{tw}:

$$y_{lat} = a_{tw}\vartheta_{tw} \qquad (2)$$

The twist stiffness is defined as the ratio between the torque and the rotation about the twist axis:

$$k_{tw} = \frac{M_{tw}}{\vartheta_{tw}} = \frac{Fa_{tw}}{\vartheta_{tw}} \qquad (3)$$

Substituting rotation ϑ_{tw} in equation (2), the expression for the calculation of the twist stiffness from static tests is obtained:

$$k_{tw} = \frac{Fa_{tw}^2}{y_{lat}} = k_{lat}a_{tw}^2 \qquad (4)$$

Actually, the system shown in Figure 1 is well suited for static tests, but it shows some limits in dynamic tests: the connection between the stem of the hydraulic actuator and the swingarms alters the behavior of the motorcycle components; moreover, the actuator cannot operate above 50 Hz. For these reasons, in order to perform dynamic tests, a different technique has been adopted: the hydraulic actuator has been removed, the swingarms have been excited by means of a hammer for modal testing and the motion of the reference plate has been measured by means of three accelerometers. The dynamic tests aim to identify at the various frequencies the deformation pattern of the swingarm, which is described by means of the dynamic twist axis. When the frequency of excitation coincides with a natural frequency of the swingarm the deformation pattern coincides with the mode of vibration and the dynamic twist axis becomes the modal twist axis [15].

Experimental measurements included also a preliminary modal analysis of the swingarms, aimed to identify the natural frequencies of the bending and torsion modes and their damping coefficients. Modal analysis has been performed exciting the motorcycle components by means of a hammer impact and measuring the vibrations by means of a tri-axial accelerometer. The axes of the accelerometer were oriented as follows: x-axis aligned with the travel direction (pointing backwards), z-axis aligned with the vertical direction (pointing upwards) and y-axis as the vector product between x and z. Vibrations have been measured on 18 points for swingarm 1 and 6 points for swingarm 2, whereas the impact has been exerted on the rear wheel hub. Experimental frequency response functions (FRFs) have been calculated as the ratios between the cross-spectrum of input signal (force) and output signal (acceleration) and the auto-spectrum of input signal; for each point, the average of three different measurements has been examined.

2.2 Tests on swingarm 1

The moduli of the FRFs measured on swingarm 1 are shown in Figure 2. Three large peaks are evident in the range 0-300 Hz. The first peak corresponds to the bending mode of the swingarm (in which the two arms move in the y direction), whereas the second peak corresponds to the torsion mode of the motorcycle component (in which the two arms move in opposition in the z direction). The third peak is due to the longitudinal mode of the swingarm (the two arms move in the z direction) This is an in-plane mode of the vehicle, which is not interesting in the framework of this research that focuses on out-of-plane stability.

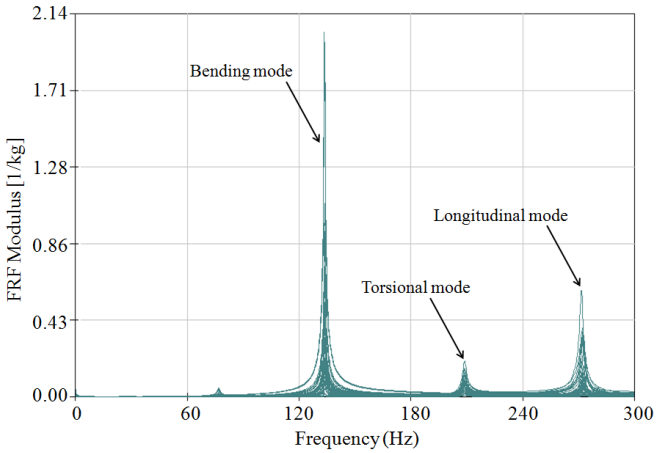

Figure 2. Overlays of FRFs measured on swingarm 1.

Figure 3 shows the results of the tests carried out on swingarm 1 for the identification of the static and dynamic twist axes. The black thick line is the static twist axis, the black thick point is the point where the force has been applied and the small red points are the points in which the displacement has been measured by means of the laser sensors. The static twist axis is almost orthogonal to the swingarm and intersects the motorcycle component rather close to the stiff column of the testing rig (swingarm pivot). Shifting the attention to the dynamic twist axes in resonance conditions, it is interesting to notice that the dynamic twist axis identified at the natural frequency of the bending mode is very close to the static twist axis and crosses the swingarm almost orthogonally, because the swingarm chiefly vibrates in the lateral direction. On the contrary, at the natural frequency of the torsion mode, the dynamic twist axis is almost orthogonal to the previous one and parallel to the swingarm.

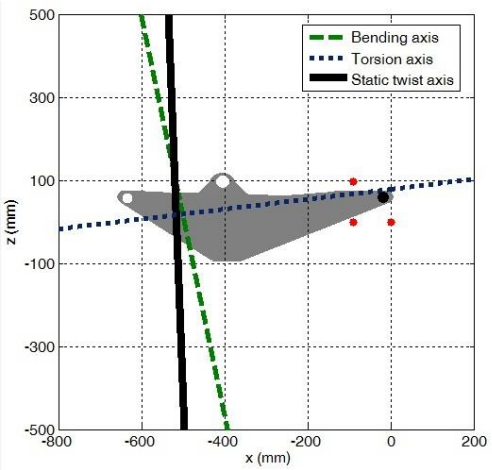

Figure 3. Static and dynamic twist axes of swingarm 1.

2.3 Tests on swingarm 2

Figure 4 shows the overlay of the FRFs measured on swingarm 2. Also for this swingarm, three resonance frequencies are evident in the range 0-300 Hz.

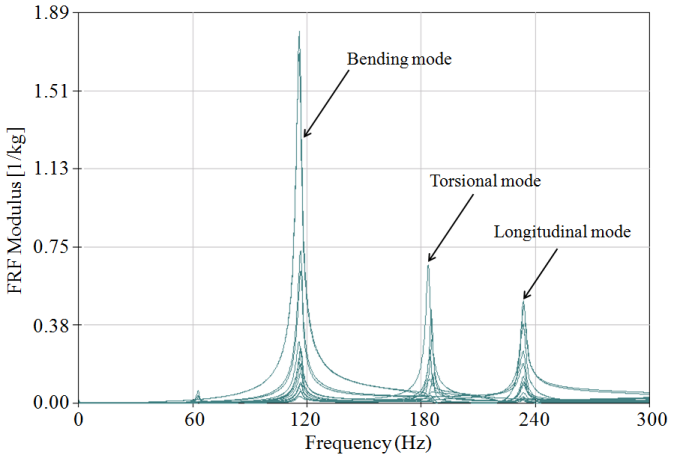

Figure 4. Overlays of FRFs measured on swingarm 2.

Figure 5 shows the results of the tests carried out on swingarm 2 for the identification of the static and dynamic twist axes. The static twist axis intersects the swingarm at about one third of its length and is almost orthogonal to its major axis. This result is in satisfactory agreement with the theory of solid mechanics about the twist axis of a cantilever beam locked at one end and loaded by a static force at the free end [14], it confirms that this swingarm can be approximated as a cantilever beam due to its simple geometry. Coming to the dynamic twist axis, at the natural frequency of the bending mode the axis crosses the swingarm almost orthogonally; at the natural frequency of the torsion mode, on the contrary, the dynamic twist axis is almost parallel to the swingarm.

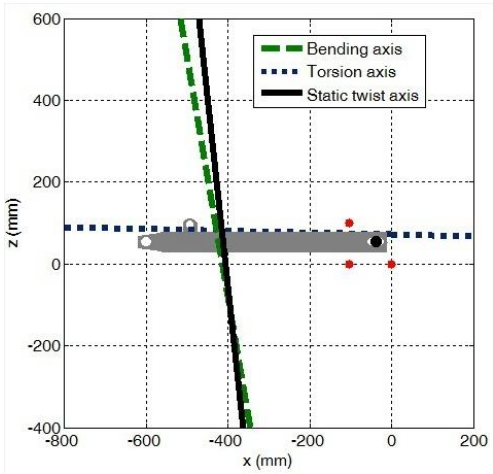

Figure 5. Static and dynamic twist axes of Swingarm 2.

2.4 Mass properties

In order to have a more realistic model of the swingarm in the motorcycle model, the mass properties have been measured by means of laboratory tests. The center of gravity (CoG) has been measured on a specific testing rig equipped with four load cells which support the motorcycle component under testing, as shown in Figure 6. The machine can be tilted from 0° to 30° with a step increment angle of 3°. For each angle the output of the load cells is recorded and the collected data are processed in order to identify the CoG position according to the reference system shown in figure 6. Assuming xz-plane as a symmetry plane of the swingarm, the y-coordinate of the center of gravity is equal to zero.

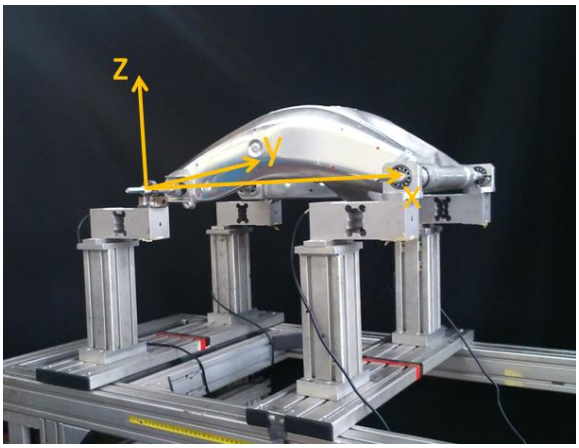

Figure 6. Swingarm 1 on the machine for the identification of the CoG.

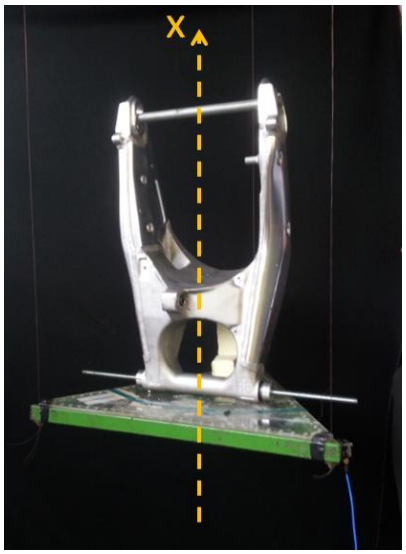

Figure 7. Swingarm 1 on the trifilar pendulum.

For the calculation of the moments of inertia of the swingarms, a trifilar pendulum has been used as shown in figure 7. The pendulum consists of a plate hung to a frame by means of three stiff wires. If the inertial characteristics of the plate are known, it is possible to identify the moment of inertia of the swingarm about the vertical axis of the pendulum from the measurement of the natural frequency of the pendulum about the vertical axis. Different setups of the swingarm on the plate make it possible to measure the moments of inertia about different axes. The following table summarizes the geometric and inertial characteristics of the two swingarms that have been tested.

Table 1. Geometric and inertial properties of the swingarms.

	Mass	**CoG Position**		**Moments of inertia about CoG**		
	m(kg)	**x(mm)**	**z(mm)**	**Ixx (kgm^2)**	**Iyy (kgm^2)**	**Izz (kgm^2)**
Swingarm 1	6.96	0.299	0.027	0.11	0.27	0.34
Swingarm 2	5.45	0.196	0.015	0.08	0.21	0.28

3 Identification of lumped stiffness and damping coefficients

3.1 Stiffness decomposition

The static and modal twist axes of the swingarms can be identified by means of the measurements techniques described in the previous sections. Then it is possible to decompose the twist stiffness into the bending and torsion components that will be introduced in the model of the swingarm for numerical simulations. Under the assumption of small rotations, stiffness decomposition is carried out according to two basic properties:

a) The lateral displacement of the swingarm due to a rotation about the twist axis is equal to the sum of the displacements caused by the rotations about the bending and the torsion axes.
b) The rotation of the reference plate about twist axis is equal to the sum of rotations of this rigid body about bending and torsion axes.

Property a) leads to the following equation:

$$y_{lat} = \vartheta_{tw} a_{tw} = \vartheta_b a_b + \vartheta_t a_t \qquad (5)$$

in which, ϑ_{tw}, ϑ_b and ϑ_t are twist, bending and torsion angles, a_{tw}, a_b and a_t are twist, bending and torsion arms, which can be calculated from the measured positions of the static and dynamic twist axes. Since twist, bending and torsion angles are given by:

$$\vartheta_{tw} = F\frac{a_{tw}}{k_{tw}} \quad \vartheta_b = F\frac{a_b}{k_b} \quad \vartheta_t = F\frac{a_t}{k_t} \qquad (6)$$

equation (5) becomes:

$$\frac{a_{tw}^{\,2}}{k_{tw}} = \frac{a_b^{\,2}}{k_b} + \frac{a_t^{\,2}}{k_t} \qquad (7)$$

Property b) leads to the following equations:

$$\vartheta_{tw}\cos(\beta) = \vartheta_b \cos(\beta_b) + \vartheta_t \cos(\beta_t) \qquad (8)$$

$$\vartheta_{tw}\sin(\beta) = \vartheta_b \sin(\beta_b) + \vartheta_t \sin(\beta_t) \qquad (9)$$

in which β is the angle from *x* axis to static twist axis, β_b is the angle from *x* axis to the twist axis of the bending mode and β_t is the angle from *x* axis to the twist axis of the torsion mode, see figure 8.
If equations (6) are introduced into equations (8) and (9) and the ratio between these equations is calculated, equation (10) is obtained, which correlates the angle of the static twist axis with the angles of the modal twist axes:

$$\tan(\beta) = \frac{\frac{a_b}{k_b}\sin(\beta_b) + \frac{a_t}{k_t}\sin(\beta_t)}{\frac{a_b}{k_b}\cos(\beta_b) + \frac{a_t}{k_t}\cos(\beta_t)} \qquad (10)$$

Bending and torsion stiffnesses can be calculated solving the system of equations (7) and (10).

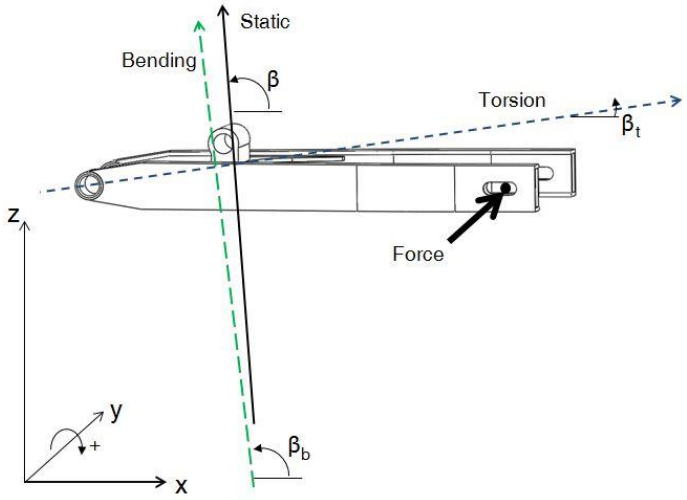

Figure 8. Stiffness decomposition.

Tables 2 and 3 summarize the identified static and dynamic properties of the swingarms.

Table 2. Static and dynamic properties of swingarm 1.

Static properties	
Linear stiffness	1083 kN/m
Twist arm	0.477 m
Twist stiffness	246.4 kNm/rad
Bending arm	0.451 m
Bending stiffness	222.4 kNm/rad
Torsion arm	0.026 m
Torsion stiffness	77.4 kNm/rad
Dynamic properties	
Bending mode	134 Hz
Hysteretic damping	0.74 %
Torsion mode	208 Hz
Hysteretic damping	0.97 %

Table 3. Static and dynamic properties of swingarm 2.

Static properties	
Linear stiffness	623 kN/m
Twist arm	0.375 m
Twist stiffness	87.6 kNm/rad
Bending arm	0.388 m
Bending stiffness	94.2 kNm/rad
Torsion arm	0.014 m
Torsion stiffness	55.2 kNm/rad
Dynamic properties	
Bending mode	115 Hz
Hysteretic damping	1.73 %
Torsion mode	184 Hz
Hysteretic damping	1.02 %

It is worth highlighting that the twist axis in pure bending conditions could be evaluated by applying a lateral force on the elastic axis of the swingarm, which is the locus of the points of application of a lateral force that produces deflection without torsion; but the determination of the elastic axis requires some specific tests. The twist axis in pure torsion condition could be identified by applying a torque to the swingarm, but, again, specific testing equipment is needed. The decomposition method based on the modal twist axes does not require specific equipment, but the axes of the bending and torsion modes do not coincide exactly with the axes that can be found by means of static tests. This happens because in actual structures the bending-dominated mode includes also some torsion deformation and the torsion-dominated mode includes some bending deformation.

A closer inspection of the identified stiffness values of swingarm 1 highlights that the twist stiffness is larger than the bending and torsion stiffnesses. Actually, this result is due to the fact that the stiffness are referred to different axes, according to the experimental measurements. In order to compare the stiffnesses in the proper way, they have to be referred to the same axis. When a multibody system is characterized by linear kinematic relations, stiffness about an axis (k) can be reduced to an equivalent stiffness (k') about another axis, making use of the ratio of velocities (τ) about the two axes [16]:

$$k' = \tau^2 k \qquad (11)$$

For the bending and twist axes the velocity ratio τ can be calculated considering that twist velocity and bending velocity have to give the same lateral velocity of the wheel:

$$\dot{\vartheta}_b a_b = \dot{y}_{lat} = \dot{\vartheta}_{tw} a_{tw} \qquad (12)$$

Hence:

$$\tau_b = \frac{\dot{\vartheta}_b}{\dot{\vartheta}_{tw}} = \frac{a_{tw}}{a_b} \qquad (13)$$

and reduced bending stiffness becomes:

$$k_b' = \frac{a_{tw}^2}{a_b^2} k_b \qquad (14)$$

In a similar way torsion stiffness can be reduced to the twist axis:

$$k_t' = \frac{a_{tw}^2}{a_t^2} k_t \qquad (15)$$

Global stiffness about the twist axis can be considered as the series of reduced bending and torsion stiffnesses:

$$\frac{1}{k_{tw}} = \frac{1}{k_b'} + \frac{1}{k_t'} \qquad (16)$$

If equations (14) and (15) are introduced in (16) the following relation between reduced stiffnesses is obtained:

$$\frac{1}{k_{tw}} = \frac{1}{\frac{a_{tw}^{\ 2}}{a_b^{\ 2}} k_b} + \frac{1}{\frac{a_{tw}^{\ 2}}{a_t^{\ 2}} k_t} \qquad (17)$$

Table 4 shows the values of bending and torsion stiffness reduced about the twist axis: the twist stiffness is lower than its components.

Table 4. Reduced stiffness values for swingarms 1 and 2.

	k_{tw} (kNm/rad)	k_b' (kNm/rad)	k_t' (kNm/rad)
Swingarm 1	246.4	248.8	26050
Swingarm 2	87.6	88	39600

It is worth highlighting that if both sides of equation (17) are multiplied by $a_{tw}^{\ 2}$, equation (7) is obtained again.

3.2 Damping coefficient identification

Since the bending and torsion modes are well separated in frequency, the damping coefficients c_b and c_t can be identified by means of a 1DOF approach:

$$c_b = 2\zeta_b\sqrt{k_b J_b} \qquad c_t = 2\zeta_t\sqrt{k_t J_t} \qquad (18)$$

in which J_b and J_t are the moment of inertia of the swingarm about the bending and torsion axes and ζ_b and ζ_t are the viscous damping ratios. From the equation of the natural frequency f of a 1DOF system, the moment of inertia can be calculated as:

$$J = \frac{k}{(2\pi f)^2} \qquad (19)$$

Equation (19) can be introduced in the formula for the identification of the damping coefficient, which becomes:

$$c_b = \frac{k_b\zeta_b}{\pi f_b} \qquad c_t = \frac{k_t\zeta_t}{\pi f_t} \qquad (20)$$

in which the natural frequency and the viscous damping are known from modal analysis results (the viscous damping is equal to half of the measured hysteretic damping).

Equations (18) cannot be employed for the identification of the damping coefficient about the static twist axis because the twist stiffness has been identified by means of static tests and no natural frequency and damping coefficient have been measured. For this reason, in order to identify the coefficient c_{tw}, an energy approach has been adopted. According to the law of conservation of energy, the work dissipated for performing a rotation about the twist axis must be equal to the sum of the work dissipated for performing rotations about the bending and torsion axes, according to the following equation:

$$W_{tw} = W_b + W_t \qquad (21)$$

Considering that the work is equal to the viscous moment multiplied by the rotational displacement, the equation (21) becomes:

$$c_{tw}\dot{\vartheta}_{tw}\delta\vartheta_{tw} = c_b\dot{\vartheta}_b\delta\vartheta_b + c_t\dot{\vartheta}_t\delta\vartheta_t \qquad (22)$$

If we isolate c_{tw}, the previous equation becomes:

$$c_{tw} = c_b\frac{\dot{\vartheta}_b\delta\vartheta_b}{\dot{\vartheta}_{tw}\delta\vartheta_{tw}} + c_t\frac{\dot{\vartheta}_t\delta\vartheta_t}{\dot{\vartheta}_{tw}\delta\vartheta_{tw}} \qquad (23)$$

Since twist, bending and torsion angles are given by equation (6), it is possible to calculate the following ratios:

$$\frac{\vartheta_b}{\vartheta_{tw}} = \frac{a_b k_{tw}}{k_b a_{tw}} \qquad \frac{\vartheta_t}{\vartheta_{tw}} = \frac{a_t k_{tw}}{k_t a_{tw}} \qquad (24)$$

which hold true also for velocities and differential rotations since a_b, a_{tw}, k_b, k_{tw} are constant. Introducing equations (24) into equation (23), c_{tw} is calculated:

$$c_{tw} = c_b\left(\frac{a_b k_{tw}}{k_b a_{tw}}\right)^2 + c_t\left(\frac{a_t k_{tw}}{k_t a_{tw}}\right)^2 \qquad (25)$$

The identified damping coefficients are summarized in Table 5.

Table 5. Identified damping coefficients for swingarms 1 and 2.

	c_b (Nms/rad)	c_t (Nms/rad)	c_{tw} (Nms/rad)
Swingarm 1	1.97	0.58	2.18
Swingarm 2	2.25	0.49	2.09

4 Numerical simulations

In order to understand the effect of swingarm deformabilities on motorcycles stability, the FastBike multibody code has been used; more details about this software can be found in [17]. Two different numerical models have been built, considering that the tested swingarms are mounted on different motorcycles. In particular, swingarm 1 has been inserted in the model of a super-sport motorcycle, whereas swingarm 2 has been inserted in the model of an enduro motorcycle. The main parameters of the analyzed vehicles are reported in the Table 6. The rider is assumed to be a rigid body stiffly attached to the saddle. Both models have 9 degrees of freedom (DOF) related to the gross motion of the motorcycle: the position and orientation of the chassis (6 DOFs), the steer rotation (1 DOF), the wheels rotations (2 DOFs).

Other degrees of freedom are added to simulate the structural flexibilities measured by means of laboratory tests. In particular, for each motorcycle four cases are taken into account: model with rigid swingarm, model 1 with a rotation DOF about the bending axis to represent bending deformability, model 2 with a rotation DOF about the torsion axis to represent torsion deformability and, finally, model 3 with a rotation DOF about the twist axis to represent twist deformability.

Table 6. Motorcycle parameters used in the models.

	Supersport	**Enduro**
Mass of the whole motorcycle	166.2 kg	190.4kg
Rider mass	77.5 kg	77.5 kg
Height of the centre of gravity from the ground (vehicle + rider)	0.672 m	0.697m
Longitudinal position of the centre of gravity, from rear contact point (vehicle + rider)	0.698 m	0.623m
Wheelbase	1.430 m	1.497m
Caster Angle	23.7°	29.8°
Normal trail	0.086 m	0.104 m
Roll moment of inertia (vehicle + rider)	26.7 kg m^2	33.4 kg m^2
Pitch moment of inertia (vehicle + rider)	51.0 kg m^2	64.9 kg m^2
Yaw moment of inertia (vehicle + rider)	28.1 kg m^2	39.4 kg m^2
Product of inertia (vehicle + rider)	3.2 kg m^2	1.98 kg m^2
Front rolling radius	0.315 m	0.321m
Front tire cornering stiffness per unit load	12.3 rad^{-1}	9.09 rad^{-1}
Front tire camber stiffness per unit load	1.24 rad^{-1}	1.67 rad^{-1}
Front tire self-aligning moment stiffness per unit load	-0.45 m rad^{-1}	-0.44 m rad^{-1}
Front tire twisting moment stiffness per unit load	0.032m rad^{-1}	0.035 m rad^{-1}
Rear rolling radius	0.300 m	0.289 m
Rear tire cornering stiffness per unit load	10.1 rad^{-1}	11.8 rad^{-1}
Rear tire camber stiffness per unit load	1.52 rad^{-1}	1.71 rad^{-1}
Rear tire self-aligning moment stiffness per unit load	-0.47 m rad^{-1}	-0.22 m rad^{-1}
Rear tire twisting moment stiffness per unit load	0.054 m rad^{-1}	0.038 m rad^{-1}

The simulations have been performed at speed ranging from 0 to 40 m/s for the enduro motorcycle and from 0 to 50 m/s for the super sport bike, with an increment of 1 m/s per step for both simulations; the limited top speed is related to the power train characteristics of the motorcycles.

The stability analysis test is divided into three phases. In the first phase, the motorcycle trim is computed by solving the non-linear equations of the model for the chosen dynamics conditions (with a speed range from 0 to 40 m/s or from 0 to 50 m/s depending on the model considered, with no longitudinal or lateral acceleration). The second phase consists in transforming the non-linear equations into linear equations resulting in a state-space matrix. The standard formula for the linear system is:

$$\dot{x} = Ax + Bu \tag{26}$$

The last phase is the calculation of the eigenvalues of state-space matrix A.

Frequency (f) and damping ratio (ξ) are calculated from the real part (real) and the imaginary part (imag) of the eigenvalues of each vibration mode:

$$f = \frac{imag}{2\pi}$$

$$\xi = -\frac{real}{\sqrt{real^2 + imag^2}} \tag{27}$$

Simulations results are collected in terms of root-loci in which the x coordinate is the real part of the eigenvalue, whereas the y coordinate is the natural frequency, see Figure 9. For the four cases described above, weave and wobble modes are plotted in the graphs. The arrows show the direction of increasing speed.

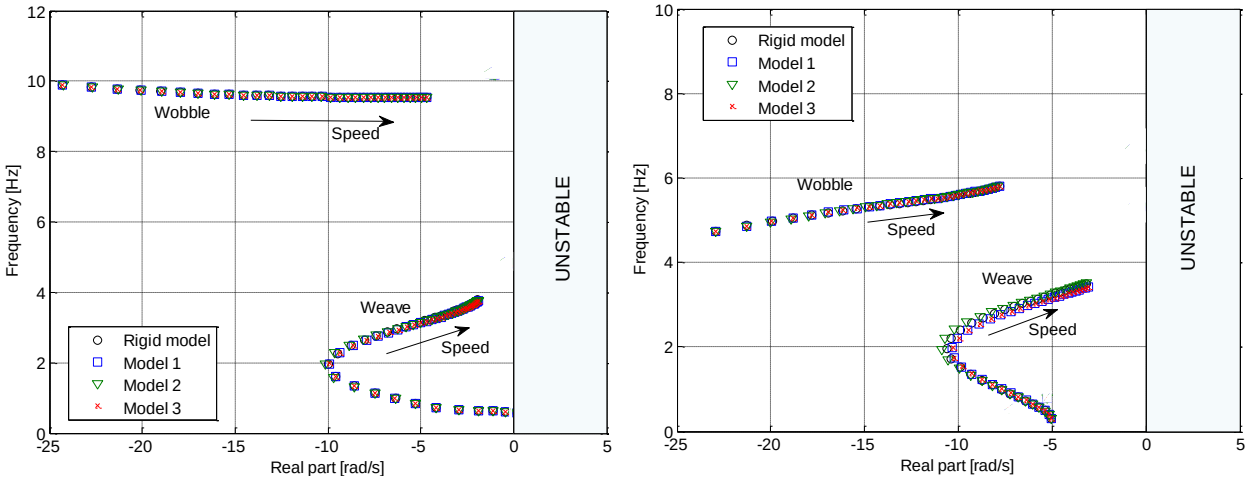

Figure 9.Root-loci: super-sport (1) vs. enduro (2) motorcycle.

In both graphs, weave and wobble modes are clearly evident. Focusing on the root-locus of the super-sport motorcycle, the wobble mode occurs at about 10 Hz, it is stable in the whole range of investigated speeds and its frequency is not significantly affected by the speed of the vehicle. The weave mode occurs at lower frequencies (about 0.5-4 Hz), it is unstable for very low speeds, which are not realistic in normal riding conditions, and it is stable in the remaining speed range. No effect due to the introduction of swingarm structural deformability can be observed on the wobble mode, since the wobble involves only the front frame of the motorcycle. On the contrary, swingarm compliances affect the weave mode, actually the effect is not strong if compared to the rigid model, owing to the high stiffness values of the super-sport swingarm.

Coming to the root-locus of the enduro motorcycle, the wobble mode occurs at a lower frequency due to different tires and inertial properties of the enduro motorcycle and it is more affected by the speed of the vehicle. The weave mode occurs at about 0.5-3.5 Hz and it is stable in the whole speed range. As for the super-sport motorcycle, no effect due to swingarm deformability can be observed on the wobble mode. On the contrary, the effects of swingarm deformability on the weave mode are more evident, owing to the larger differences in terms of stiffness between the rigid model and the models that include torsion, bending and twist compliances.

The modes due to the introduction of swingarm structural deformability are not shown in the graphs because they occur at high frequencies: for the super-sport model the bending mode appears at about 52 Hz and the torsional mode appears at 65 Hz; for the enduro models they occur at about 38 and 60 Hz, respectively.

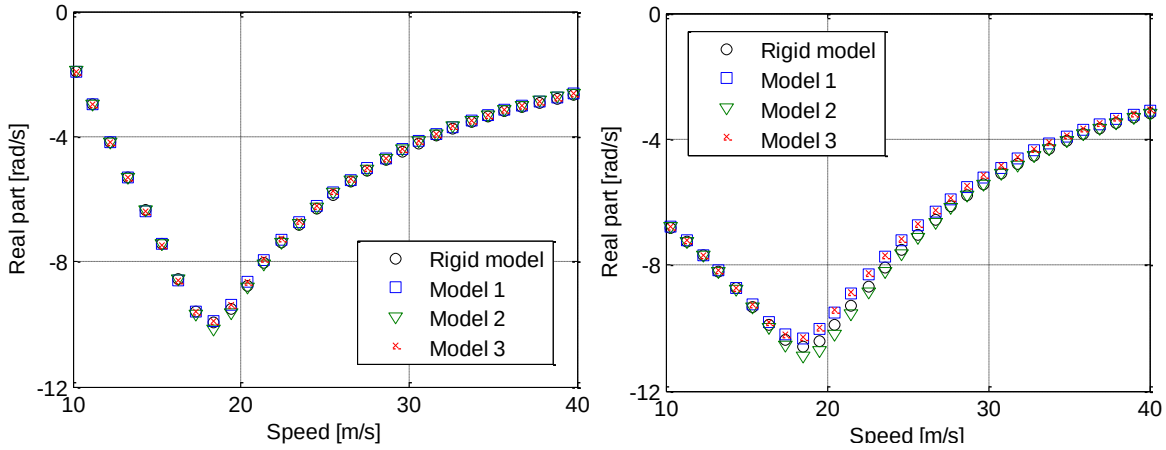

Figure 10. Real part of weave mode for the super-sport (left) and enduro (right) motorcycles for speed from 10 to 40 m/s.

Figure 10 highlights the effects of the swingarm deformability on the real part of the eigenvalue (i.e. on the stability) of the weave mode for speeds in the range 10-40 m/s. Similar trends can be observed in both motorcycles, the enduro (right) shows larger variations than the super sport (left). At low speed (up to 17 m/s), the four models present no significant differences in the stability behaviour; from 17 to 26 m/s, the model 2 is the most stable while model 1 and 3 are the least stable. Increasing the speed, the effects of the structural deformability tend to disappear and the modulus of the real part decreases with a tendency towards instability.

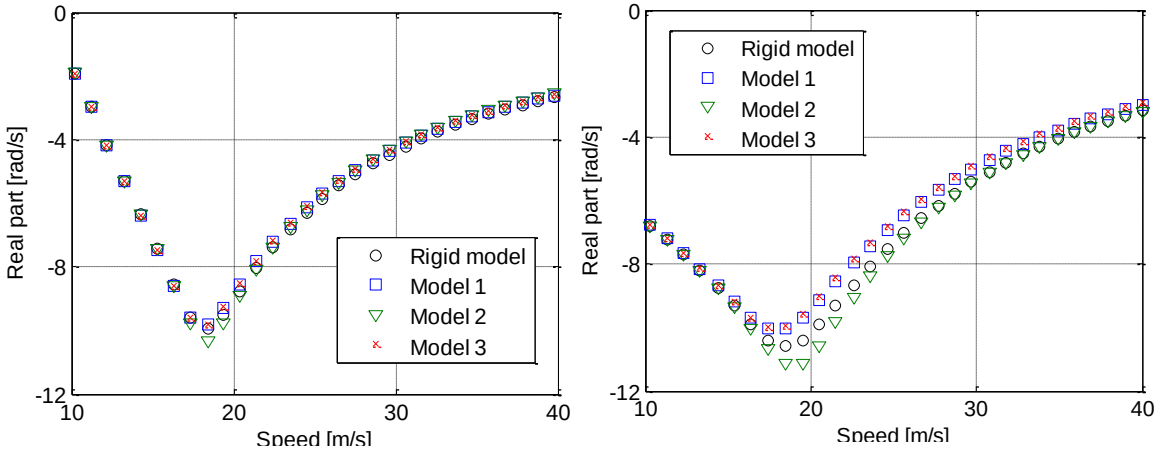

Figure 11. Real part of weave mode for the super-sport (left) and enduro (right) motorcycles for speed from 10 to 40 m/s, (doubled compliances).

In order to emphasize the effect of structural deformability on the weave mode, the experimental stiffness values have been halved. Damping coefficient has been divided by $\sqrt{2}$, in order to maintain the same damping ratio according to (18). Figure 11 shows the results of the simulations: the general trend of the models is the same of Figure 10, but the curves exhibit larger percentage variations of the real part with respect to the rigid model, especially in the range 17-26 m/s.

For both motorcycles the maximum stability of weave occurs at about 18 m/s and the maximum effect of swingarm deformability appears around this speed.

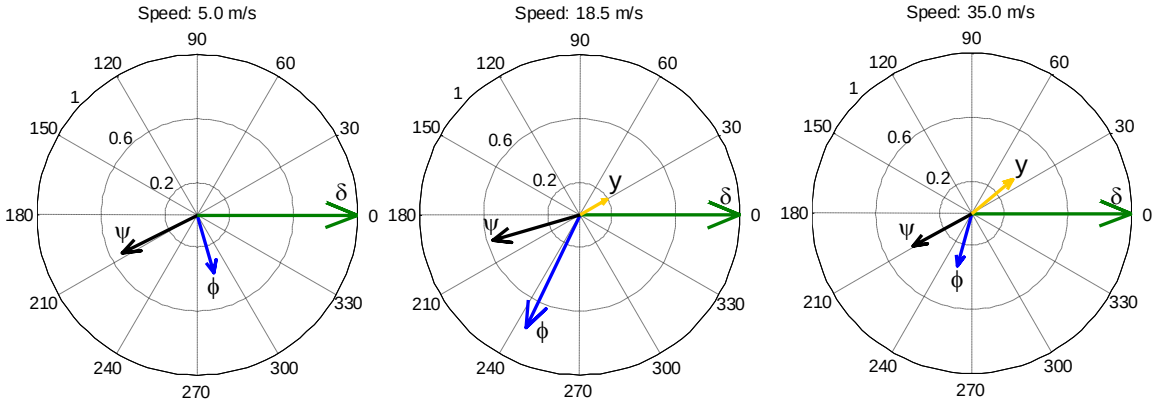

Figure 12. Modal shapes of the weave mode for the enduro motorcycle (model with torsion deformability).

In order to understand the reason of this behaviour, the modal shapes of the weave mode of the enduro motorcycle at three forward speeds have been represented by means of compass plots (Figure 12), in which each modal component is represented by a vector.

The amplitudes of the rotations have been normalized with respect to the largest one and the phase of the steering angle has been set to 0°. Under the assumption of small displacements, the lateral displacement has been converted into an angle by normalizing it with respect to the wheelbase of the motorcycle. In agreement with [4] and [5] the yaw angle ψ is almost in opposition with respect to the steer angle δ and the roll angle φ is almost 90° out-of-phase with respect to the steer angle; the amplitude and the phase of the lateral displacement increase with the speed. Torsion component is not represented, since it modulus is much smaller than the others, nevertheless it reaches the largest amplitude at 18.5 m/s.

From the point of view of vehicle stability, it is worth highlighting that at the speed of maximum stability (18.5 m/s) the amplitudes of roll, yaw and torsion components of weave mode reach their maximum. Therefore it is possible that the stiffness and damping characteristics of the swingarm have the largest effect on stability at 18.5 m/s because at this speed the weave mode involves the swingarm more than at other speeds.

It is interesting to notice that, at this speed, the model with torsion deformability is the most stable, this phenomenon can be caused by the torsion gyroscopic effect that has been found in scooters [10]. In motorcycles this effect can be larger than in scooters, owing to the larger ratio between the spin moment of inertia of the wheel and the moment of inertia of the swingarm about the twist axis.

5 Concluding remarks

The value and the position of the lumped element stiffness that represents the deformability of a swingarm have been evaluated by means of a simple static test carried out on a test bench that has been developed according to the twist axis concept. Dynamic tests carried out by means of standard equipment for modal testing have made it possible to identify the torsion and bending components of swingarm stiffness and to evaluate swingarm damping. There are very few data about swingarm stiffness in the literature, the stiffness values identified in the present research are in agreement with the ones reported by other authors [1] [18] [19] [20] and, as predictable, larger than the ones of scooters [10].

The identified stiffness and damping values have been implemented in the multibody models of a super sport and an enduro motorcycle and specific simulations have been carried out to highlight the effect of the various components of swingarm deformability. Results show that swingarm deformability has a small effect on the stability of super sport motorcycles, but has an interesting effect on the stability of the weave mode of enduro motorcycles in a specific range of speeds.

References

[1] Cossalter V. Motorcycle Dynamics second edition, Lulu.com, (2007).

[2] Sharp RS. The stability and control of motorcycles, Journal of Mechanical Engineering Science (1971), Vol. 13 n.5.

[3] Cossalter V, Lot R and Maggio F. The influence of tire properties on the stability of a motorcycle in straight running and curves, Proceedings of the 2002 SAE Automotive Dynamics and Stability Conference, (2002).

[4] Cossalter V, Doria A, Lot R and Massaro M. The effect of rider's passive steering impedance on motorcycle stability: identification and analysis, Meccanica (2011), 46, pp. 279-292.

[5] Doria A, Formentini M and Tognazzo M. Experimental and numerical analysis of rider motion in weave conditions, Vehicle System Dynamics (2012), 50(8), pp. 1247–1260.

[6] Cossalter V., Doria A., Lot R. Steady turning of two wheeled vehicles, Vehicle System Dynamics (1999), vol 31, pp 157- 181.

[7] Lot R. A motorcycle tire model for dynamic simulations: theoretical and experimental aspects, Meccanica (2004), 39, pp. 207-220.

[8] Doria A and Taraborrelli L. Out-of-plane vibrations and relaxation length of the tyres for single-track vehicles, Proc IMechE Part D: J Automobile Engineering (2016), 230(5), pp. 609–622

[9] Sharp RS. and Alstead CJ. The influence of structural flexibilities on the straight-running stability of motorcycles, Vehicle System Dynamics (1980), 9, pp. 327–357.

[10] Cossalter V, Lot R and Massaro R. The influence of frame compliance and rider mobility on the scooter stability, Vehicle System Dynamics (2007), 45(4), pp. 313–326.

[11] Lake K, Thomas R and Williams O. The influence of compliant chassis components on motorcycle dynamics: "An historical overview and the potential future impact of carbon fibre", Vehicle System Dynamics (2012), 50(7), pp. 1043-1052.

[12] Cossalter V, Doria A, Massaro M and Taraborrelli L. Experimental and numerical investigation on the motorcycle front frame flexibility and its effect on stability, Mechanical Systems and Signal Processing (2015), 60-61, pp. 452–471.

[13] Giles CG. and Sharp RS. Static and dynamic stiffness and deflection mode measurements on a motorcycle, with particular reference to steering behaviour, Proc. of IMechE Conference on Road Vehicle Handling (1983), pp. 185-192.

[14] Doria A and Taraborrelli L., The twist axis of frames with particular application to motorcycles, Proceedings of the Institution of Mechanical Engineers, Part C: Journal of Mech. Engineering Science 2016, Vol. 230(17), 3026-3039.

[15] Doria. A and Taraborrelli L., Identification of the critical stiffnesses of motorcycles in static and dynamic conditions, Proceedings of the ASME 2016 International Design Engineering Technical Conferences & Computers and Information in Engineering Conference IDETC/CIE 2016 August 21-24, 2016, Charlotte, North Carolina, USA, DETC2016-59092.

[16] Blundell M and Harty D. Multibody Systems Approach to Vehicle Dynamics, Elsevier Butterworth Heinemann (2004).

[17] Cossalter V, Lot R and Massaro M. An advanced multibody code for handling and stability analysis of motorcycles, Meccanica (2011), 46(5), pp. 943-958.

[18] Smith, B and Kienhöfer F. Development of a carbon fibre swingarm, 9th South African Conference on Computational and Applied Mechanics, SACAM 2014.

[19] Airoldi A, Bertoli S, Lanzi L, Sirna M and Sala G. Design of a motorcycle composite swing-arm by means of multi-objective optimisation, Appl Compos Mater (2012), 19, pp. 599-618.

[20] Risitano G., Scappaticci L., Grimaldi C. and Mariani F., Analysis of the Structural Behavior of Racing Motorcycle Swingarms, SAE Technical Paper, 2012-01-0207, 2012, doi:10.4271/2012-01-0207.

Nomenclature

F	lateral force
y_{lat}	lateral displacement
k_{lat}	lateral stiffness
M_{tw}	twist torque
k_{tw}, k_b, k_t	twist, bending and torsion stiffnesses
a_{tw}, a_b, a_t	twist, bending and torsion arms
$\vartheta_{tw}, \vartheta_b, \vartheta_t$	twist, bending and torsion angles
τ	ratio of velocities
β	angle from x axis to static twist axis
β_b, β_t	angles from x axis to the dynamic axes of the bending mode and the torsion mode
c_{tw}, c_b, c_t	damping coefficients
J_b, J_t	moment of inertia of the swingarm about the bending and torsion axes
ζ_b, ζ_t	viscous dampings
W_{tw}, W_b, W_t	work dissipated for performing a rotation about the twist bending or torsion axis

List of captions